

THE COMPTON-THICK SEYFERT 2 NUCLEUS OF NGC 3281: TORUS CONSTRAINTS FROM THE 9.7 μ m SILICATE ABSORPTION

Dinalva A. Sales¹; M. G. Pastoriza^{1,2}; R. Riffel¹; C. Winge³; A. Rodríguez-Ardila⁴; A. C. Carciofi⁵

dinalva.aires@ufrgs.br

ABSTRACT

We present mid infrared (Mid-IR) spectra of the Compton-thick Seyfert 2 galaxy NGC 3281, obtained with the Thermal-Region Camera Spectrograph (T-ReCS) at the Gemini South telescope. The spectra present a very deep silicate absorption at 9.7 μ m, and [SIV] 10.5 μ m and [Ne II] 12.7 μ m ionic lines, but no evidence of PAH emission. We find that the nuclear optical extinction is in the range $24 \leq A_V \leq 83$ mag. A temperature $T = 300$ K was found for the black-body dust continuum component of the unresolved 65 pc nucleus and at 130 pc SE, while the region at 130 pc reveals a colder temperature (200 K). We describe the nuclear spectrum of NGC 3281 using a clumpy torus model that suggests that the nucleus of this galaxy hosts a dusty toroidal structure. According to this model, the ratio between the inner and outer radius of the torus in NGC 3281 is $R_0/R_d = 20$, with 14 clouds in the equatorial radius with optical depth of $\tau_V = 40$ mag. We would be looking in the direction of the torus equatorial radius ($i = 60^\circ$), which has outer radius of $R_0 \sim 11$ pc. The column density is $N_H \approx 1.2 \times 10^{24} \text{ cm}^{-2}$ and iron K α equivalent width ($\approx 0.5 - 1.2$ keV) are used to check the torus geometry. Our findings indicate that the X-ray absorbing column density, which classifies NGC 3281 as a Compton-thick source, may also be responsible for the absorption at 9.7 μ m providing strong evidence that the silicate dust responsible for this absorption can be located in the AGN torus.

Subject headings: galaxies: Seyfert - infrared: ISM - ISM: molecules - techniques: spectroscopic

1. Introduction

Mid-infrared (Mid-IR) spectra of active galactic nuclei (AGNs) are rich in emission features, such as polycyclic aromatic hydrocar-

bons (PAHs), molecular hydrogen and prominent forbidden emission lines (Sturm et al. 2000; Weedman et al. 2005; Wu et al. 2009; Gallimore et al. 2010; Sales et al. 2010). Another spectral feature commonly observed in AGNs is silicate at $\sim 9.7 \mu$ m and 18 μ m, both in emission and absorption.

The AGN unified model proposes the existence of a dense concentration of absorbing material surrounding the central engine in a toroidal distribution, which blocks the broad line region (BLR) emission from the line of sight in Seyfert 2 (Sy 2) galaxies (Antonucci 1993). However, it is not yet clear if the molecular gas and dust detected in Mid-IR spectra is actually associated with the absorbing material required by the so-called torus in

¹Departamento de Astronomia, Universidade Federal do Rio Grande do Sul. Av. Bento Gonçalves 9500, Porto Alegre, RS, Brazil

²Conselho Nacional de Desenvolvimento Científico e Tecnológico, Brazil

³Gemini Observatory, c/o Aura, Inc., Casilla 603, La Serena, Chile

⁴Laboratório Nacional de Astrofísica/MCT, Rua dos Estados Unidos 154, Itajubá, MG, Brazil

⁵Instituto de Astronomia, Geofísica e Ciências Atmosféricas, Universidade de São Paulo, Rua do Matão 1226, Cidade Universitária, São Paulo, SP, Brazil

the unified model.

Hao et al. (2007) studied the distribution of the silicate feature strengths in a sample of 196 AGNs and ultraluminous infrared galaxies (ULIRGs). They found that the spectra of quasars and Seyfert 1 (Sy 1) galaxies are characterized by silicate features in emission, with few Sy 1s presenting weak absorptions. In contrast, Sy 2 spectra are dominated by weak silicate absorption. These results suggest that the silicate emission (or absorption) is related to the line of sight, in the framework of the AGN unified model. In addition, most of the ULIRGs show very deep silicate absorption (Hao et al. 2007).

The silicate behavior in AGNs can be explained using Nenkova’s torus models (Nenkova et al. 2002, 2008a,b), which consider an ensemble of individual clouds instead of the standard “solid doughnut”. Mason et al. (2006) detected the silicate emission feature in the Sy 2 galaxy NGC 2110, and compared it with the Nenkova et al. (2008b) clumpy torus models, demonstrating that the presence of silicate emission can also be explained by an edge-on clumpy distribution. From their best-fit model, they conclude that there would be a small number of clouds along the line of sight, with a distribution that does not extend far above the torus equatorial plane.

According to Hao et al. (2007) the presence of strong silicate absorption and the absence of PAH features in some active galaxies, can be interpreted as extremely heavily obscuration in these sources. An example of such an object is NGC 3281. Its spectrum shows a very deep silicate absorption at $9.7 \mu\text{m}$, as well as the forbidden emission lines [S III] $18.7 \mu\text{m}$, [S IV] $10.5 \mu\text{m}$, [Ne II] $12.8 \mu\text{m}$, [Ne III] $15.5 \mu\text{m}$, [Ne V] $14.3 \mu\text{m}$ and $24.3 \mu\text{m}$, [Ne VI] $7.6 \mu\text{m}$ and [O IV] $25.8 \mu\text{m}$. No PAH emission was detected in the Spitzer spectrum (Wu et al. 2009). In addition, NGC 3281 is a luminous infrared galaxy ($\log L_{IR} \sim 10.73 L_{\odot}$, Sanders et al. 2003), classified as a Sy 2. Its optical spectrum was studied by Storchi-Bergmann et al. (1992), finding that the kinematics of the kpc extended ionized gas can be described by rotation in a plane, with material outflowing ($v \sim 150 \text{ km s}^{-1}$) from the nucleus within a conical structure. They also suggest that NGC 3281 has dust asymmetrically distributed with respect to the ionized gas.

In addition, using Advanced Satellite for Cosmology and Astrophysics (*ASCA*) data, Simpson (1998) found that NGC 3281 shows an extremely complex X-ray spectrum, with a prominent iron emission line and a large absorbing column density ($N_H \sim 7.1 \pm 1.2 \times 10^{23} \text{ cm}^{-2}$) that when combined with the nuclear extinction inferred from the near-infrared color analysis ($A_V = 22 \pm 11 \text{ mag}$), results in a N_H/A_V ratio one order of magnitude higher than that of the Galaxy (Bohlin et al. 1978). This effect was attributed to an optically thick material along the line of sight of both the X-ray and the infrared emitting regions, which obscures the entire X-ray source but only a fraction of the much larger IR emitting region. Later, Vignali & Comastri (2002) using the Italian-Dutch satellite *BeppoSAX*, found a N_H/A_V ratio about twice that derived by Simpson (1998), adding NGC 3281 to the list of AGNs presenting dust properties different from the Galaxy. The difference in the N_H/A_V values derived by both studies, according to Vignali & Comastri (2002), is due to the limited *ASCA* band-pass. Vignali & Comastri (2002) also show that its X-ray spectrum ($E < 10 \text{ keV}$) is reflection-dominated, with a relatively strong $K\alpha$ iron emission line and a heavily absorbed nuclear continuum ($N_H \simeq 1.5 - 2 \times 10^{24} \text{ cm}^{-2}$). Hence, they classify NGC 3281 as a Compton-thick galaxy. The high values found for the absorption column density in NGC 3281 also explain the extremely high ratio $F_{[O III]}/F_{2-10 \text{ keV}} \approx 0.3$, when compared to the average (≈ 0.02) value obtained for a sample of Sy 2 galaxies (Mulchaey et al. 1994).

It follows from the above discussion that this galaxy has a very heavily obscured nucleus, which makes it a key object to study whether or not the observed dust absorption is associated with the dusty torus of the unified model. Thus, it may provide unambiguous observational evidence of this structure. We present in this paper ground bases Mid-IR high-angular resolution spectra of the galaxy NGC 3281. The Thermal-Region Camera Spectrograph (T-ReCS; Telesco et al. 1998) attached to the Gemini South telescope give a spatial resolution of 16 pc/pix , which is very adequate to study the dust distribution in the $\sim 200 \text{ pc}$ central radius of this galaxy. This paper is structured as follows: in Section 2 we describe the observa-

tion and data reduction processes. Results are discussed in Section 3. Summary and conclusion are presented in Section 4.

2. Observations and Data Reduction

Ground-based Mid-IR observations of NGC 3281 were obtained with the T-ReCS in queue mode at Gemini South, in 2009 April 06 UT, as part of program GS-2009A-Q-34. Conditions were clear, with water vapor column in the range 5–8mm, and image quality of $0''.33$ in the N band, as measured from the acquisition images of the telluric standards observed right before and/or after the science frames. All observations used a standard chop-nod technique to remove time-variable sky background, telescope thermal emission, and the effect of $1/f$ noise from the array/electronics. The slit was oriented along $PA = 315^\circ$, with a chop throw of $15''$, oriented along $PA = 225^\circ$, perpendicular to the slit direction, in order to include only the signal of the guided beam position in the frame and avoid possible nod effects in the spatial direction. The same slit position/nod orientation were used for the telluric standards. The instrument configuration used the low-resolution ($R \sim 100$) grating and the $0''.36$ slit, for a dispersion of $0.0223 \mu\text{m}/\text{pixel}$ and a spectral resolution of $0.08 \mu\text{m}$. The pixel scale is $0.089 \text{ arcsec}/\text{pixel}$ in the spatial direction, and the slit is $21''.6$ long. Spectral coverage was of $7.1 \mu\text{m}$ centered at $10.5 \mu\text{m}$. The total on-source integration time was 980 sec.

The data reduction was performed using the MIDIR and GNIRS sub-packages of Gemini IRAF¹ package. To extract the final spectrum, we combined the chop- and nod-subtracted frames using the tasks TPREPARE and MISTACK in the MIDIR package. Wavelength calibration was obtained from the sky lines in the raw frames. To remove the telluric absorption lines from the galaxy spectrum, we divided the extracted spectrum for each observing night by that of the telluric standard stars HD 3438 or HD 4786 (Cohen et al. 1999), observed before and/or after the science target. Finally, the spectrum was flux calibrated by inter-

polating a black-body function to the spectrum of the telluric standard. For this step we used the task MSTELLURIC in the MIDIR package.

Fig. 1a shows the slit superposed on the NGC 3281 N-band acquisition image. Panel b of this figure illustrates the slit on the narrow [O III] maps taken from Schmitt et al. (2003b). Panel c shows that the N-band galaxy luminosity profile is extended with respect to that of the N-band stellar profile of HR3438.

We extracted seven one dimensional (1D) spectra: one centered in the unresolved nucleus (4-pixel = 0.36 arcsec , which corresponds to $\sim 65 \text{ pc}$ for a distance of 43 Mpc, using $H_0 = 74 \text{ km s}^{-1} \text{ Mpc}^{-1}$), plus extractions centered at 130 pc, 195 pc and 260 pc to the Northwest (NW) and Southeast (SE) directions. Deep silicate absorption is observed at the nucleus and at 130 pc in both NW and SE directions of the nucleus (Fig. 2). The extraction at 195 pc NW shows a weak absorption. The remaining extraction does not present silicate absorption. Therefore, we can conclude that the dust is concentrated inside a radius of 200 pc.

3. Results and Discussion

3.1. The Mid-IR Spectra

The NGC 3281 T-ReCS spectra (Fig. 2) clearly show that a deep silicate absorption, as well as the [S IV] $10.5 \mu\text{m}$ and [Ne II] $12.7 \mu\text{m}$ emission lines, are observed up to 130 pc from the nucleus. In addition, PAH emission bands are not detected in the spectra, in agreement with the Spitzer spectrum (Wu et al. 2009). As discussed in the introduction, NGC 3281 is one exception among Sy 2 galaxies, as most ($\sim 80\%$) of the objects in this class present PAH emission bands and no deep silicate absorption in their Mid-IR spectra (Sales et al. 2010).

In order to estimate the silicate absorption apparent strength (S_{sil}), we use the definition of Spoon et al. (2007):

$$S_{sil} = \ln \frac{f_{obs}(9.7 \mu\text{m})}{f_{cont}(9.7 \mu\text{m})}, \quad (1)$$

where f_{obs} is the observed flux density and f_{cont} is the observed mid-line pseudo-continuum flux density. To determine the S_{sil} , we avoid telluric

¹IRAF is distributed by the National Optical Astronomy Observatory, which is operated by the Association of Universities for Research in Astronomy (AURA) under cooperative agreement with the National Science Foundation.

bands and emission line regions, using the same methodology as Mason et al. (2006). The values derived from the four spatial positions where the silicate absorption is observed are shown in column 7 of Tab. 1.

For the unresolved nucleus, we obtain $S_{sil} = -1.3 \pm 0.1$. Similar values of S_{sil} are observed in ULIRGs, while much weaker (average is -0.61) absorptions are seen in Sy 2s (see Fig.2 of Hao et al. 2007). The remaining three extraction have similar values to that of the nucleus.

When dealing with dusty sources, a more physical parameter is the line of sight depth (τ), which can be estimated from S_{sil} at $9.7 \mu\text{m}$ using the equation $\ln(e^{-\tau_{9.7}}) = -\tau_{9.7} = \frac{f_{obs}(9.7 \mu\text{m})}{f_{cont}(9.7 \mu\text{m})}$ (Nenkova et al. 2008b). Furthermore, we can derive the apparent optical extinction using $A_V^{app} = \tau_{9.7} \times 18.5 \pm 2 \text{ mag}$ (Draine 2003). The resulting values are shown in Tab. 1. The dust extinction for the unresolved nucleus of NGC 3281 is $A_V^{app} = 24 \pm 5 \text{ mag}$, in agreement with the value ($A_V = 22 \pm 11 \text{ mag}$) derived by combined IR data (Simpson 1998). Peruse that our uncertainties is much lower than these authors. We note from the values listed in Tab. 1 that the position labeled as 1 (130 pc from the nucleus at NW direction) presents a slightly higher extinction than the central one ($A_V = 28 \pm 8 \text{ mag}$).

To estimate in a more robust way the line of sight depth at $9.7 \mu\text{m}$ ($\tau_{9.7}$) in NGC 3281 we used the PAHFIT² code (Smith et al. 2007), which assumes that the source spectrum is composed by continuum emission from dust and starlight, prominent emission lines, individual and blended PAH emission bands, and that the light is attenuated by extinction due to silicate grains. PAHFIT models the extinction using the dust opacity law of Kemper et al. (2004), where the infrared extinction is considered as a power law plus silicate features peaking at $9.7 \mu\text{m}$. For details see Smith et al. (2007).

We used this approach to determine the contribution of the distinct components to the spectral energy distribution (SED) of NGC 3281 as a function of the distance to the galaxy centre. As the spectra do not show PAH emission, we have not included this component in the fitting. The

other input parameters are the same as those used by Sales et al. (2010), which are appropriate for AGNs. The results of the decomposition of the NGC 3281 spectra are shown in Fig. 3, and the derived silicate optical depths are given in Tab. 1.

Clearly, $\tau_{9.7}$ varies along the slit, being $\tau_{9.7} = 4.5 \pm 0.7$ at the unresolved nucleus and $\tau_{9.7} = 4.6 \pm 0.7$ at 130 pc NW extraction. In constrast, it reaches $\tau_{9.7} = 5.5 \pm 0.8$ for the 130 pc SE extraction. The dust extinction (A_V) values estimated using the PAHFIT derived line of sight depth, column 10 in Tab. 1, are much larger than those obtained from the S_{sil} . The latter are obtained from the depth at $9.7 \mu\text{m}$ while the PAHFIT code takes the whole profile of the silicate absorption feature into account, thus the S_{sil} indicator should be taken as a lower limit for the A_V . The obtained opacity values were compared to those of the Seyfert sample from Gallimore et al. (2010). The histogram of $\tau_{9.7}$ (Fig. 5) shows that the dust opacity in NGC 3281 is one of the highest observed in Seyfert galaxies.

The thermal dust continuum components required to fit the observed spectra of the unresolved nucleus and 130 pc SE is a black-body with $T = 300 \text{ K}$, while the 130 pc NW spectrum requires it a black-body of $T = 200 \text{ K}$. This colder region has the deepest silicate absorption, consequently is more heavily obscured ($A_V = 102 \pm 26 \text{ mag}$) than the nucleus and the SE region. The presence of this obscuring material is consistent with the spatial distribution of the optical reddening found by Storchi-Bergmann et al. (1992). Note that our slit position is perpendicular to the cone observed in [O III]. See their Fig. 9 and 2.

In order to get additional support of that highly reddened region, we overplot the T-ReCS slit position on the [O III] $\lambda 5007 \text{ \AA}$ maps taken from Schmitt et al. (2003b). We found that the 130 pc NW region coincide with a region where [O III] emission is not observed in agreement with those previously found from X-ray data. That is, the NGC 3281 is a heavily obscured source.

²Source code and documentation for PAHFIT are available at <http://tir.astro.utoledo.edu/jdsmith/research/pahfit.php>

3.2. Is the observed silicate absorption detected at the unresolved nucleus associated with the dusty torus required by the unified AGN model?

There are several torus models, some authors take it as having an uniform dust density distribution (e.g. Pier & Krolik 1992; Granato et al. 1997; Siebenmorgen et al. 2004; Fritz et al. 2006). However, for dust grains to survive in the torus environment, they should be formed by clumpy structures (Krolik & Begelman 1988), and new models have been developed where the dust grains are distributed in a clumpy medium (e.g. Nenkova et al. 2002, 2008a,b; Hönig et al. 2006). Therefore, we compare the uncontaminated nuclear spectrum (see below) with theoretical SED obtained from Nenkova’s models (e.g. Nenkova et al. 2002, 2008a,b).

In their modeling³, Nenkova et al. assume that the dusty material surrounding the AGN is distributed in clumps forming a toroidal geometry, and determine the following parameters: *i*) the number of clouds N_0 in the torus equatorial radius; *ii*) the optical depth for an individual cloud in the V band (τ_V); *iii*) the radial extension of the clumpy distribution, $Y = R_0/R_d$, where R_0 and R_d are the outer and inner radius of the torus, respectively; *iv*) the power law index q that describes the radial density profile ($\propto r^{-q}$); *v*) the torus angular width, constrained by a Gaussian angular distribution of σ ; *vi*) the observed viewing angle i .

In order to properly analyze the spectrum from the nuclear dusty structure, it is necessary to first remove the host galaxy contribution. For this, we have subtracted from the central aperture the spectrum obtained from averaging the two adjacent extractions (apertures -1 and 1, Fig. 1). Noise effects are reduced by smoothing (with a rectangular box of size 5 pixels) the final spectrum. The emission lines were removed by simple interpolation and the region where the telluric band is located (Fig.2) were not used in the fit. Then, the smoothed spectrum was compared with the $\sim 10^6$ CLUMPY theoretical SEDs, and the best fit is obtained by searching for the minimum in the equation:

$$\chi^2 = \frac{1}{N} \sum_{i=1}^N \left(\frac{F_{obs, \lambda_i} - F_{mod, \lambda_i}}{\delta_{\lambda_i}} \right)^2, \quad (2)$$

where N is the number of data points in the spectrum, F_{obs, λ_i} , F_{mod, λ_i} and δ_{λ_i} are the observed, theoretical fluxes at each wavelength and their respective uncertainties. The later were taken as being 10% of F_{λ} , which are the expected ones for T-ReCS observations (Radomski et al. 2002; Mason et al. 2006). Note that both F_{obs, λ_i} and F_{mod, λ_i} were normalized to unit at $9.0\mu\text{m}$, with the uncertainties being properly propagated. The parameter set that provides the best fit is shown in Table 2, and the corresponding theoretical SED is over-plotted on the NGC 3281 decontaminated nuclear spectrum (Fig. 4). Due to the very large number of models required to cover the parameter space, we estimate the uncertainties for the best model following the approach of Mason et al. (2009, see also Nikutta et al. (2009)), but instead of using only the three best models, we calculated the mean and standard deviation for the parameters considering all models with a χ^2 value within 10% of the best-fitting result (76 in total). The locus of the corresponding theoretical SEDs is plotted as a grey region in Figure 4. Our approach is similar to that used by Nikutta et al. (2009), thus, we have also tested other χ^2 deviation fractions (5%, 10%, 15% and 20%, corresponding to 17, 76, 151 and 291 acceptable solutions, respectively). In general our technique produce similar results than that obtained by Nikutta et al. (2009), however, our methodology tends to produce a locus with less acceptable solutions than Nikutta’s one. The mean parameters derived with the different χ^2 deviations are shown in Table 2.

The physical parameters of the best-fit model to the nuclear uncontaminated SEDs suggest that NGC 3281 hosts a dusty toroidal structure. The dusty clouds, each with an optical depth $\tau_V = 40\text{mag}$, occupy a toroidal volume with $R_0/R_d = 20$. The distribution of the clouds follows a power-law radial behavior ($r^{-1.5}$), and the number of clouds along the equatorial radius is 10. The angular distribution of the clouds is characterized by a width $\sigma = 70^\circ$. These results are in agreement with the unified AGN model, which requires the presence of a dusty structure that obscures the broad line region in Sy 2 galaxies. From the fitted

³The models are available from <http://www.pa.uky.edu/clumpy/>

models we would be looking in a direction nearby of the torus equator ($i = 60^\circ$)

In general, the torus parameters derived here are similar to those obtained by Ramos Almeida et al. (2009), except for the number of clouds and optical depth per single cloud, where they find only 5 clouds with $\tau_V = 10$ in the equatorial radius. This discrepancy can be due to the different constraints available, as Ramos Almeida et al. (2009) used Mid-IR photometric data (see also Ramos Almeida et al. 2011; Alonso-Herrero et al. 2011), while the data presented here would allow for a more detailed description of the spectral behavior of the silicate dust, thus providing a better input to the modeling procedure.

The Nenkova et al. (2008b) models adopt a standard dust-to-gas ratio, and assume the column density of a single cloud to be $N_H \sim 10^{22} - 10^{23} \text{ cm}^{-2}$. In addition, the total number of clouds at a viewing angle i is given by a Gaussian distribution: $N_{obs}(i) = N_0 \exp\left[-\left(\frac{90-i}{\sigma}\right)^2\right]$, thus resulting in a column density of $N_H^{(obs)} = N_{obs}(i) N_H$ at the observer view angle. Using the above, we can then derive a column density of $N_H \approx 1.2 \times 10^{24} \text{ cm}^{-2}$ for the uncontaminated nuclear spectrum of NGC 3281, which is consistent with the values derived by Vignali & Comastri (2002) from X-ray observations ($\sim 2 \times 10^{24} \text{ cm}^{-2}$).

Moreover, Levenson et al. (2002) demonstrated that for heavily obscured AGN the iron $K\alpha$ EW values depend on the torus geometry. We compare the torus geometrical parameters derived in our paper with those of Levenson et al. (2002), and found that the present torus aperture ($\sigma = 70^\circ$) correspond to $\theta = 20^\circ$ in the Levenson et al. (2002)'s models. The observer view angle has the same definition for both models ($i = 60^\circ$). From Figure 2 of Levenson et al. (2002) and using the above parameters we estimate that the iron $K\alpha$ EW for NGC 3281 is $\approx 2 - 3 \text{ keV}$, which is in agreement with that found by Vignali & Comastri (2002), confirming their results, that this galaxy would show a large EW for the iron $K\alpha$ line. We point out that this torus geometry was inferred from the silicate absorption line, this indicates that the X-ray absorbing column density, which makes NGC 3281 a Compton-thick source, may also be responsible for the absorption at $9.7 \mu\text{m}$. Therefore, our re-

sults provide strong evidence that the silicate dust responsible for such absorption is located in the AGN torus. Following Nenkova et al. (2008b), and adopting a dust sublimation temperature of 1500K, we estimate a torus outer radius of $R_0 \sim 11 \text{ pc}$. This value is consistent with the results of Jaffe et al. (2004); Tristram et al. (2007) and Ramos Almeida et al. (2009).

We also derive the intrinsic bolometric luminosity for the AGN from the best-fit model, finding $L_{bol} = 1.9 \times 10^{45} \text{ erg s}^{-1}$. This value agrees with the intrinsic luminosity obtained by Vignali & Comastri (2002) from X-ray data, when applying the conversion factor suggested by Elvis et al. (2004), resulting $L_{X-ray}^{bol} \approx 3.2 \times 10^{44} \text{ erg s}^{-1}$. We note that NGC 3281 has a high X-ray luminosity when compared to objects studied by Ramos Almeida et al. (2009).

4. SUMMARY AND CONCLUSIONS

In this work we present high-spatial resolution Mid-IR spectra of the Compton-thick Sy 2 galaxy NGC 3281. The ground-based Mid-IR data were taken with the T-ReCS spectrograph, and our main results can be summarized as follows.

- NGC 3281's spectra show a very deep silicate absorption, as well as [S IV] $10.5 \mu\text{m}$ and [Ne II] $12.7 \mu\text{m}$ ionic lines. However, the spectra do not present PAH emission bands, which makes this galaxy uncommon among the Sy 2s class (Sales et al. 2010). Furthermore, the dust is concentrated inside a radius of 200 pc.
- The optical extinction, A_V , of the nucleus and its neighborhood was estimated using the S_{sil} indicator and PAHFIT code. From the S_{sil} indicator we infer the nuclear dust extinction $A_V^{app} = 24 \pm 2 \text{ mag}$, while the PAHFIT code provides $A_V = 83 \pm 22 \text{ mag}$. We point out that the first value can only be used as a lower limit. This large extinction confirms that this galaxy, if compared with Gallimore et al. (2010)' Seyfert sample (83 sources), is a heavily obscured source compatible with a Compton-thick galaxy scenario.
- The black-body temperature due to dust continuum components for the unresolved

nucleus and the region at 130 pc SE is $T = 300$ K. A colder black-body ($T = 200$ K) was found for the region at 130 pc NW, which also has the highest derived visual extinction ($A_V = 102 \pm 0.2$ mag).

- The nuclear uncontaminated spectrum follows a clumpy torus model (Nenkova et al. 2008b), which suggests that NGC 3281 has a dusty toroidal structure. The dusty clouds occupy a toroidal volume with $R_0/R_d = 20$, with each cloud having an optical depth $\tau_V = 40$ mag. The distribution of the clouds follows a power-law radial behavior $r^{-1.5}$ and the number of clouds in the equatorial radius is 14. The angular distribution of the clouds has width of $\sigma = 70^\circ$. These results agree with the unified AGN model that to block the broad line region emission of Sy 2 galaxies, requires a dusty structure. According to the best-fit model, we would be looking in the direction nearby of the torus equatorial radius ($i = 60^\circ$), having an outer radius of $R_0 \sim 11$ pc.
- We derive a column density of $N_H = 1.2 \times 10^{24} \text{ cm}^{-2}$ for NGC 3281 indicates that the X-ray absorbing column density, which classifies NGC 3281 as a Compton-thick source, may also be responsible for the absorption at $9.7 \mu\text{m}$. In addition, our results provide strong evidence that the silicate dust responsible for such absorption is located in the AGN torus. From Nenkova's models we find that the bolometric luminosity of this AGN is $L_{bol} = 1.9 \times 10^{45} \text{ erg s}^{-1}$, which shows that NGC 3281 is a very luminous source.

We thank an anonymous referee for helpful suggestions. Based on observations obtained at the Gemini Observatory, which is operated by the Association of Universities for Research in Astronomy, Inc., under a cooperative agreement with the NSF on behalf of the Gemini partnership: the National Science Foundation (United States), the Science and Technology Facilities Council (United Kingdom), the National Research Council (Canada), CONICYT (Chile), the Australian Research Council (Australia), Ministério

da Ciência e Tecnologia (Brazil) and Ministerio de Ciencia, Tecnología e Innovación Productiva (Argentina). We thank E. Balbinot, as well as Charles Bonatto, and A.C.C. acknowledges support from CNPq (grant 308985/2009-5) e Fapesp (grant 2010/19029-0).

REFERENCES

- Alonso-Herrero, A., Ramos Almeida, C., Mason, R., et al. 2011, ApJ, accepted
- Antonucci, R. 1993, ARA&A, 31, 473
- Bohlin, R. C., Savage, B. D., & Drake, J. F. 1978, ApJ, 224, 132
- Cohen, M., Walker, R. G., Carter, B., Hammerley, P., Kidger, M., & Noguchi, K. 1999, AJ, 117, 1864,
- Durret, F. & Bergeron, J. 1988, A&AS, 75, 273
- Draine, B. T. 2003, ARA&A, 41, 241
- Elvis, M., Risaliti, G., Nicastro, F., Miller, J. M., Fiore, F., & Puccetti, S. 2004, ApJ, 615, L25
- Fritz, J., Franceschini, A., & Hatziminaoglou, E. 2006, MNRAS, 366, 767
- Gallimore, J. F., Yzaguirre, A., Jakoboski, J., et al. 2010, ApJ, 187, 172
- Granato, G. L., Danese, L., & Franceschini, A. 1997, ApJ, 486, 147
- Hao, L., Weedman, D. W., Spoon, H. W. W., Marshall, J. A., Levenson, N. A., Elitzur, M., & Houck, J. R. 2007, ApJ, 655, L77
- Hönig, S. F., Beckert, T., Ohnaka, K., & Weigelt, G. 2006, A&A, 452, 459
- Houck, J. R., Roellig, T. L., van Cleve, J., et al. 2004, ApJS, 154, 18
- Jaffe, W., Meisenheimer, K., Röttgering, H. J. A., et al. 2004, Nature, 429, 47
- Kemper, F., Vriend, W. J., & Tielens, A. G. G. M. 2004, ApJ, 609, 826
- Krolik, J. H., & Begelman, M. C. 1988, ApJ, 329, 702

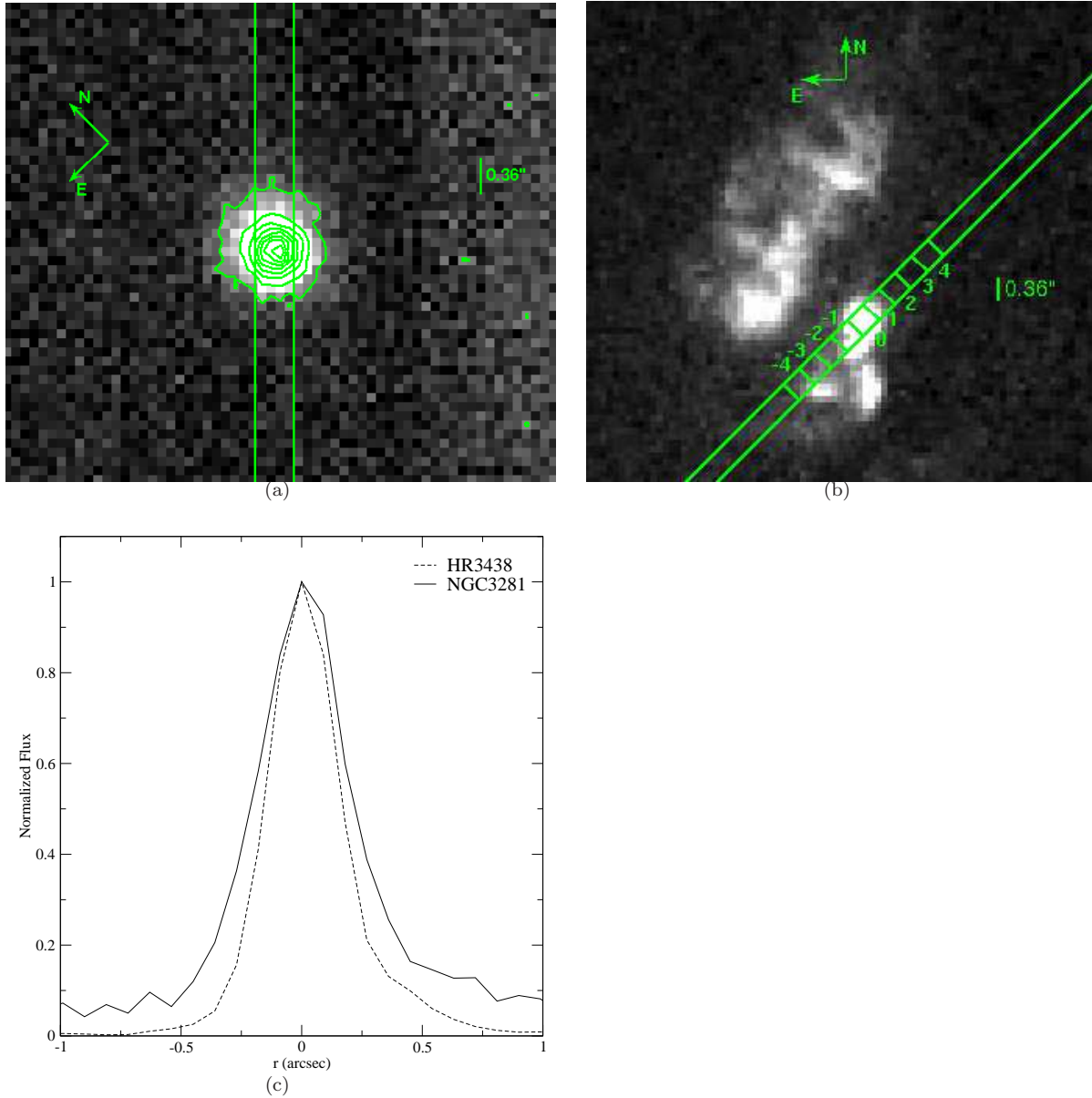


Fig. 1.— (a) The T-ReCS long-slit position overplotted on the contoured NGC3281 acquisition image. The N-band emission peak is centered in the image, which was supposed to coincide with the active nucleus. The contours are linear and stepped of 10% of the peak. (b) the slit superimposed on a $[\text{O III}]\lambda 5007 \text{ \AA}$ maps (Schmitt et al. 2003b) and spectral extraction positions were labeled. (c) the T-ReCS N-band spatial emission profile, solid and dotted lines represent the NGC 3281 galaxy and the HR3438 standard star, respectively. The fluxes are normalized to the peak value.

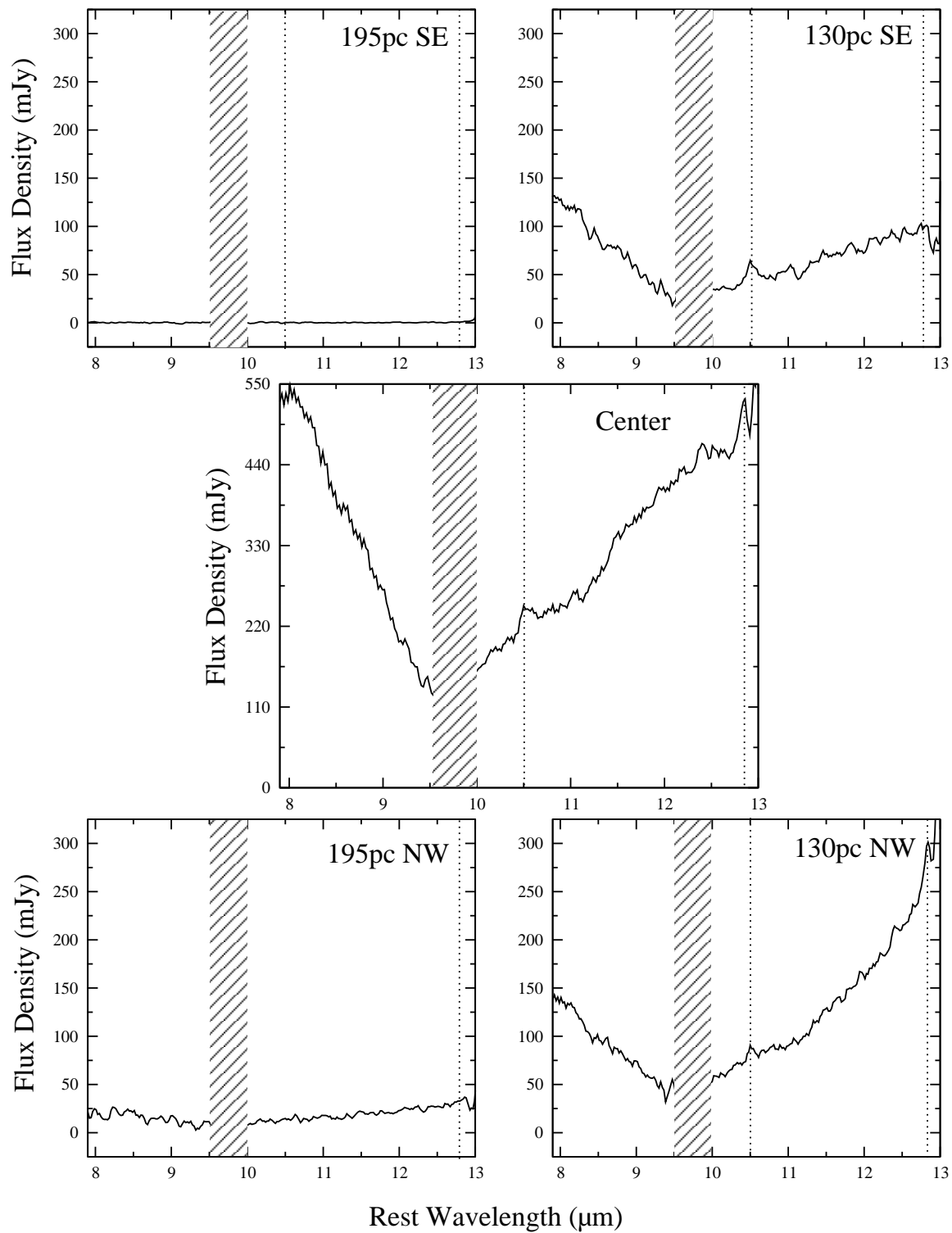


Fig. 2.— Spectra of NGC 3281 extracted in 65 pc steps along P.A. = 315°. Extraction positions are labeled, and dashed lines indicate the positions of the [S IV] 10.5 μm and [Ne II] 12.7 μm ionic lines. Telluric O₃ band is represented by the hatched area.

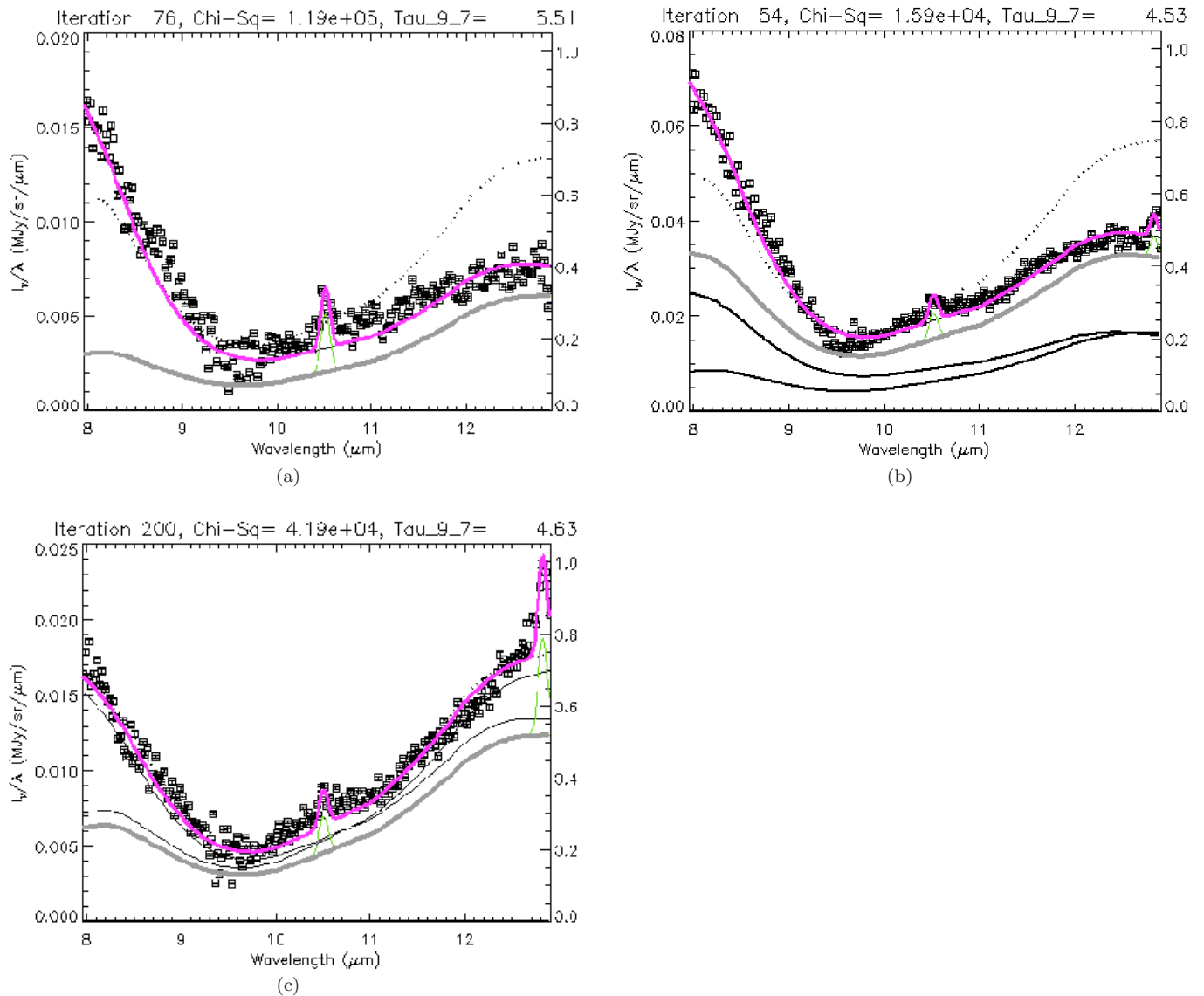


Fig. 3.— (a) The PAHFIT decomposition spectra of the 130 pc SE (-1) extraction. (b) and (c) are the same for the unresolved nucleus (0) and 130 pc NW (1) extractions, respectively. Measurements are represented by squares, uncertainties are plotted as vertical error-bars, which are smaller than the symbol size. Dotted black line indicates mixed extinction components. Solid grey and black line represent total and individual thermal dust continuum components, respectively. Green lines are emission lines. Magenta line represents the best fit model.

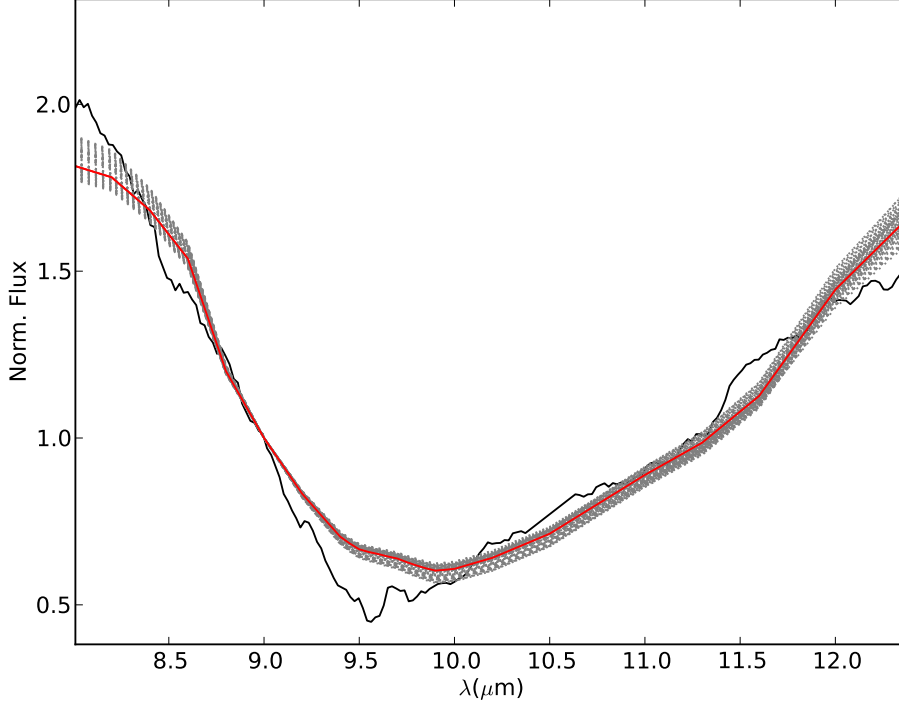


Fig. 4.— Red and grey lines are the best and 10% of best-fitting SEDs to the NGC 3281 uncontaminated spectrum, respectively. All spectra were normalized in flux at $9.0\mu\text{m}$.

TABLE 1
LINE MEASUREMENTS

Position	Label	[S IV] $_{10.5\mu\text{m}}$	EW[SIV]	[Ne II] $_{12.7\mu\text{m}}$	EW[Ne II]	S_{sil}	A_V^{app} (mag)	$\tau_{9.7}$	A_V (mag)
130 pc SE	-1	4.3 ± 0.7	0.7	-	-	-1.4 ± 0.1	26 ± 5	5.5 ± 0.8	102 ± 26
Center	0	6.2 ± 1.0	0.1	1.3 ± 0.3	0.02	-1.3 ± 0.1	24 ± 5	4.5 ± 0.7	83 ± 22
130 pc NW	1	2.3 ± 0.4	0.2	2.2 ± 0.4	0.06	-1.5 ± 0.3	28 ± 8	4.6 ± 0.7	85 ± 22
195 pc NW	2	-	-	-	-	-1.1 ± 0.1	21 ± 4	-	-

NOTE.—Columns 3 and 5 are values of the emission line integrated fluxes given in units of $10^{-16} W m^{-2}$. Columns 4 and 6 are values of the equivalent widths in units of μm . Column 7 is the silicate strengths computed from eq. 1. Column 8 shows the apparent optical extinction values derived from S_{sil} values. Column 9 is the values of optical depth inferred by PAHFIT and column 10 their optical extinction. In order to determine the optical extinction values, we assume $A_V^{app}/\tau_{sil} = 18.5 \pm 2$ (Draine 2003).

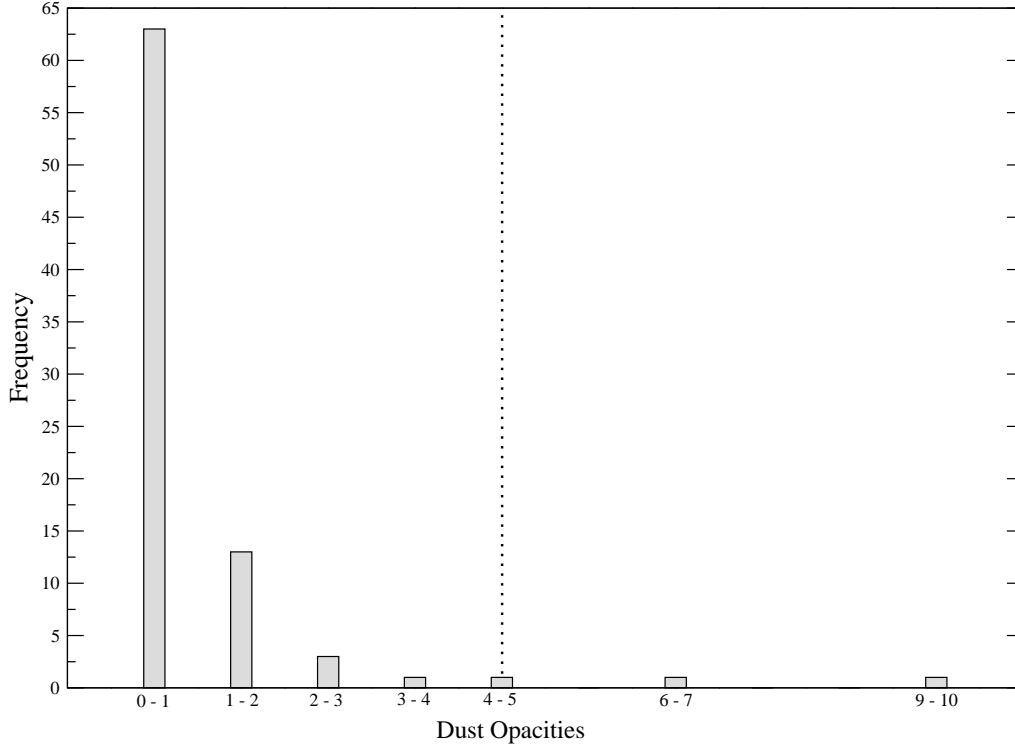


Fig. 5.— Frequency histogram of the dust opacity of the 83 Seyfert galaxies taken from Gallimore et al. (2010). Dotted line shows the value of the NGC 3281.

TABLE 2
FITTED PARAMETERS WITH CLUMPY MODEL

Parameter	Best Fit	Average 5%	Average 10%	Average 15%	Average 20%
Torus angular width (σ)	70°	$68^\circ \pm 3^\circ$	$62^\circ \pm 6^\circ$	$62^\circ \pm 7^\circ$	$61^\circ \pm 8^\circ$
Radial extent of the torus (Y)	20	20 ± 0	23 ± 4	28 ± 18	38 ± 27
Number of clouds in the torus equatorial radius (N_0)	14	13 ± 1	13 ± 2	13 ± 2	13 ± 2
Power-law index of the radial density profile (q)	1.5	1.5 ± 0	1.4 ± 0.2	1.4 ± 0.3	1.2 ± 0.5
Observers' viewing angle (i)	60°	$69^\circ \pm 11^\circ$	$76^\circ \pm 11^\circ$	$76^\circ \pm 12^\circ$	$72^\circ \pm 18^\circ$
Optical depth for individual cloud (τ_V)	40 mag	40 ± 0 mag	40 ± 0 mag	40 ± 3 mag	41 ± 8 mag
Total number of solution		17	76	151	291

NOTE.—Columns 2, 3, 4, 5 and 6 show the best value and the average for 5%, 10%, 15% and 20% of variation of the χ^2 , respectively.

- Levenson, N. A., Krolik, J. H., Życki, P. T., Heckman, T. M., Weaver, K. A., Awaki, H., & Terashima, Y. 2002, *ApJ*, 573, 81L
- Levenson, N. A., Sirocky, M. M., Hao, L., Spoon, H. W. W., Marshall, J. A., Elitzur, M., & Houck, J. R. 2007, *ApJ*, 654, 45L
- Marshall, N., Warwick, R. S., & Pounds, K. A. 1981, *MNRAS*, 194, 987
- Mason, R. E., Geballe, T. R., Packham, C., Levenson, N. A., Elitzur, M., Fisher, R. S., & Perlman, E. 2006, *ApJ*, 640, 612
- Mason, R. E., Levenson, N. A., Shi, Y., Packham, C., Gorjian, V., Cleary, K., Rhee, J., & Werner, M. 2009, *ApJ*, 693, 136L
- Mulchaey, J. S., Koratkar, A., Ward, M. J., Wilson, A. S., Whittle, M., Antonucci, R. R. J., Kinney, A. L., & Hurt, T. 1994, *ApJ*, 436, 586
- Nenkova, M., Ivezić, Ž., & Elitzur, M. 2002, *ApJ*, 570, L9
- Nenkova, M., Sirocky, M. M., Ivezić, Ž., & Elitzur, M. 2008, *ApJ*, 685, 147
- Nenkova, M., Sirocky, M. M., Nikutta, R., Ivezić, Ž., & Elitzur, M. 2008, *ApJ*, 685, 160
- Nenkova, M., Sirocky, M. M., Nikutta, R., Ivezić, Ž., & Elitzur, M. 2010, *ApJ*, 723, 1827
- Nikutta, R., Elitzur, M., & Lacy, M. 2009, *ApJ*, 707, 1550
- Phillips, M. M., Charles, P. A., & Baldwin, J. A. 1983, *ApJ*, 266, 485
- Pier, E. A., & Krolik, J. H. 1992, *ApJ*, 401, 99
- Radomski, J. T., Piña, R. K., Packham, C., Telesco, C. M., & Tadhunter, C. N. 2002, *ApJ*, 566, 675
- Ramos Almeida, C., Levenson, N. A., Rodríguez Espinosa, J. M., et al. 2009, *ApJ*, 702, 1127
- Ramos Almeida, C., Levenson, N. A., Alonso-Herrero, A., et al. 2011, *ApJ*, 731, 92
- Roche, P. F., Packham, C., Aitken, D. K., & Mason, R. E. 2007, *MNRAS*, 375, 99
- Sales, Dinalva A., Pastoriza, M. G., & Riffel, R. 2010, *ApJ*, 725, 605
- Sandage, A. 1978, *AJ*, 83, 904
- Sandage, A., & Brucato, R. 1978, *AJ*, 84, 472
- Sanders, D. B., Mazzarella, J. M., Kim, D. C., Surace, J. A., & Soifer, B. T. 2003, *AJ*, 126, 1607
- Schmitt, H. R., Ulvestad, J. S., Antonucci, R. R. J., & Kinney, A. L. 2003, *ApJS*, 132, 199
- Schmitt, H. R., Donley, J. L., Antonucci, R. R. J., Hutchings, J. B. & Kinney, A. L. 2003, *ApJS*, 148, 327
- Siebenmorgen, R., Krügel, E., & Spoon, H. W. W. 2004, *A&A*, 414, 123
- Simpson, C. 1998, *ApJ*, 509, 653
- Smith, J. D. T., Draine B. T., Dale D. A., et al. 2007, *ApJ*, 656, 770
- Spoon, H. W. W., Marshall, J. A., Houck, J. R., Elitzur, M., Hao, L., Armus, L., Brandl, B. R., & Charmandaris, V. 2007, *ApJ*, 654, 49
- Storchi-Bergmann, T., Wilson, A. S., & Baldwin, J. A. 1992, *ApJ*, 396, 45
- Sturm, E., Lutz, D., Tran, D., Feuchtgruber, H., Genzel, R., Kunze, D., Moorwood, A. F. M., & Thornley, M. D. 2000, *A&A*, 358, 481
- Telesco, C. M., Piña, Robert K., Hanna, Kevin T., Julian, Jeffrey A., Hon, David B., & Kisko, Thomas M. 1998, *Proc. SPIE*, 3354, 534
- Tristram, K. R. W., Meisenheimer, K., Jaffe, W., et al. 2007, *A&A*, 474, 837
- Vignali, C., & Comastri, A. 2002, *A&A*, 381, 834
- Young, S., Packham, C., Mason, R. E., Radomski, J. T. & Telesco, C. M. 2007, *MNRAS*, 378, 888
- Weedman, D. W., Hao, Lei, Higdon, S. J. U., et al. 2005, *ApJ*, 633, 706
- Wu, Y., Charmandaris, V., Huang, J., Spinoglio, L., & Tommasin, S. 2009, *ApJ*, 701, 658

This 2-column preprint was prepared with the AAS L^AT_EX macros v5.2.